Phosphorus-Carbon Composite for a Negative Electrode of a Sodium-ion Battery

Alexander Skundin[1,*], Dmitry Gryzlov[1], Tatiana Kulova[1], Yulia Kudryashova[1,2], Anna Kuz'mina[1]

[1] Frumkin Institute of Physical Chemistry and Electrochemistry of the RAS, 31-4 Leninskii ave., 119071 Moscow, Russia
[2] National Research University "Moscow Power Engineering Institute", 14 Krasnokazarmennaya str., 111250 Moscow, Russia.
[*]E-mail: askundin@mail.ru

Phosphorus-carbon composite was prepared by combined method consisting of grinding a mixture of red phosphorus with Ketjenblack EC300J followed by sublimation-condensation with simplified temperature scenario. The composite was characterized by XRD, EDX, SEM, and Raman-spectroscopy. The electrodes with such a composite were studied by galvanostatic cycling and cyclic voltammetry. The electrodes delivered the discharge capacity of 1870 mAh g^{-1} at C/20 and 190 mAh g^{-1} at 10C. The sodium effective diffusion coefficient in the composite was estimated as $(3-4)*10^{-14}$ cm^2 s^{-1}.

1. INTRODUCTION

The expansion of the application scale of lithium-ion batteries, as well as the creation of sodium-ion batteries require the further development of functional materials, characterized by increased values of specific capacity. Phosphorus has the highest specific capacity among materials for the negative electrodes of lithium-ion and sodium-ion batteries. The first report on the possibility of using red phosphorus as a functional material in sodium-ion batteries appeared in 2013 [1]. In this work, the possibility of achieving a reversible capacity for the sodium insertion at about 1900 mAh g^{-1} with a not too high degradation rate (0.2% per cycle) was demonstrated, and the main problems that arise when working with phosphorus are indicated, namely its insufficient electronic conductivity and appreciable volumetric expansion at the insertion of a large amount of sodium. Red phosphorus is quite stable under normal conditions. Unfortunately, its low electronic conductivity forces it to be used in the form of

composites with electronically conductive components, usually with carbon. The reversible insertion of sodium into amorphous red phosphorus proceeds according to the equation

$$P + 3Na^+ + 3e \leftrightarrow Na_3P \tag{1}$$

The value of the theoretical specific capacity for the sodium insertion (i.e., the specific capacity of the cathodic process) corresponding to this equation is 2596 mAh g^{-1}. Process (1) proceeds through a series of successive stages with the formation of intermediate sodium phosphides, including Na_3P_{11}, Na_3P_7, NaP, Na_5P_4 [2].

The literature describes a wide variety of methods for preparing amorphous red phosphorus composites with carbon, of which the most important are (*i*) simple mixing (grinding) of phosphorus and carbon powders, (*ii*) mechanochemical processing (ball-milling), (*iii*) sublimation-condensation, (*iv*) carbothermal reduction, (*v*) sol-gel and other methods of "wet chemistry".

Although many studies have shown that mechanochemical treatment [3–9] leads to much better results than simple mixing of phosphorus and carbon powders, this last technique is still used [1, 10]. Ball-milling leads both to a decrease in particle sizes and to a uniform distribution of carbon throughout the volume of the composite. Composites of red phosphorus with various forms of carbon (natural graphite, carbon black, carbon nanotubes, graphene and reduced graphene oxide) have been described [4, 5, 7, 8].

Mixing and ball-milling are simple, but not the most effective methods for creating phosphorus-carbon composites. A much more elegant method is the sublimation-condensation method with various carbon materials as a support and a special heating-cooling mode. For the first time, this method was used to prepare electrodes for a lithium-ion battery [11, 12], and as applied to sodium-ion batteries, this method was first used in 2015 in [13, 14]. In [13], single-walled nanotubes (which have better mechanical properties than multi-walled nanotubes) were chosen as the carbon material. A mixture of red phosphorus and carbon nanotubes (4:1) was sealed in a glass ampoule under vacuum. The ampoule was heated to a temperature of 600 °C and kept at this temperature for 2 hours. Then the ampoule was cooled to a temperature of 280 °C and kept at this temperature for 2 days to completely convert white phosphorus to red. The electrodes from such a composite were cycled at a current density of 50 mA g^{-1} (based on the mass of the whole composite) for 50 cycles with virtually no decrease in capacity, which amounted to about 700 mAh g^{-1}. At a current of 1 A g^{-1}, the reversible capacity was 500 mAh g^{-1}.

In [14], the carbon material was fibers doped with nitrogen. To obtain composites, a mixture of red phosphorus and such fibers was heated in a stainless steel ampoule to a temperature of 450 ° C and kept at this temperature for 3 hours. Then the ampoule was cooled to a temperature of 260 ° C and held for 18 hours. Although the phosphorus content in the initial mixture was 50%, its content in the composite, determined by thermogravimetric analysis, was only 27.5%. When cycling electrodes with such a composite with a current of 100 mA g^{-1}, their capacity decreased from 850 mAh g^{-1} in the 10th cycle to 730 mAh g^{-1} in the 55th cycle.

In [15], carbon nanotubes with a diameter of about 20 nm coated with an activated carbon layer about 50 nm thickness were used as a carbon matrix for condensing phosphorus vapor. The micropores in this layer were filled with red phosphorus, and the mesopores remained empty and were designed to dampen volume changes when sodium was inserted into phosphorus. In [16], a red phosphorus composite with ordered mesoporous carbon CMK-3 was prepared by evaporation-condensation.

To avoid the appearance of white phosphorus in the evaporation-condensation method, the authors of [17] modernized this method by introducing stepwise heat treatment. The microporous carbon YP-80F, as well as multi-walled carbon nanotubes, were used as the carbon matrix in this work. A mixture of red phosphorus and carbon material in a sealed vacuum ampoule was heated and kept at a temperature of 450 °C for 3 hours, then the ampoule was slowly (1 °C/min) cooled to a temperature of 280 °C and kept at this temperature for 24 hours. After that, the ampoule was again heated to a temperature of 340 °C, kept at this temperature for 2 h and then slowly (0.2 °C/min) cooled to a temperature of 190 °C. With further cooling to room temperature, the rate of temperature change was no longer controlled.

An original method for the synthesis of phosphorus – carbon composites using deep cooling was proposed in [18]. In accordance with this method, at first, a fraction of phosphorus nanoparticles 100–150 nm in size is selected by flotation of a suspension of red phosphorus powder in water. Then an aqueous suspension of a mixture of this fraction with graphene oxide is prepared. Ultrasonic treatment of this suspension delaminates graphene oxide into separate sheets. Then this suspension is treated with liquid nitrogen, while graphene oxide sheets are twisted, which capture phosphorus nanoparticles inside the resulting scrolls. Thus, particles of a phosphorus composite with graphene oxide with the structure of pods are obtained. The final operation is the reduction of graphene oxide with hydrazine hydrate vapors. The electrodes with such a composite containing 52% phosphorus were stably cycled at a current of 250 mA g^{-1} for 150 cycles; the specific capacity was 2355 mAh g^{-1} of phosphorus. Even at a current density of 4 A g^{-1}, the capacity was about 1000 mAh g^{-1} of phosphorus.

In [19], similar graphene scrolls composites, in which red phosphorus particles were encapsulated, were used as a precursor for the synthesis of the main composite. A polypyrrole coating was deposited from the vapor phase on this precursor. The resulting material was sealed in an ampoule with argon and held for 20 min at a temperature of 400 °C, after which it was quickly cooled (quenching). With this heat treatment, carbonization of polypyrrole and redistribution of phosphorus over the volume of the composite took place (gas phase transfer). Despite the significant complication of the synthesis compared to [18], the result obtained showed characteristics close to those of the material obtained in [18].

A similar approach to the creation of composites of red phosphorus with graphene (more precisely, with reduced graphene oxide) was described in [20]. Here, a mixture of red phosphorus with reduced graphene oxide (in a ratio of 3:1) was sealed in a vacuum quartz ampoule and kept at a temperature of 600 °C for 15 minutes, and then at a temperature of 280 °C for 10 hours. Such a simplified evaporation-condensation procedure was enough to obtain a composite with quite acceptable characteristics. At a current density of about 1600 mA g^{-1}, the capacity of such an electrode decreased over 300 cycles from 1100 to 900 mAh g^{-1}.

In [21], a combined method of manufacturing a composite of red phosphorus with carbon was used. Here, first, a mixture of phosphorus, carbon black and carbon nanotubes was ball-milled, and then it was subjected to heat treatment in a sealed ampoule under vacuum at a temperature of 455 °C for 12 hours. The resulting material was stably cycled for 200 cycles at a current of 150 mA g^{-1}, but with a rather small capacity of about 300 mAh g^{-1}. Various versions of the synthesis of red phosphorus and carbon composites by evaporation-condensation are also described in [22–26].

Herein we report a simpler method of phosphorus-carbon composite fabrication and present the properties of the composite prepared as a negative electrode for a sodium-ion battery.

2. EXPERIMENTAL

2.1 Synthesis and characterization of the material.

For the preparation of the composite, commercial powders of red phosphorus (Ruskhim OJSC) and carbon black (Ketjenblack EC300J, AkzoNobel Chemicals Inc.) were used. The composite was prepared by the combined method (mixing and grinding in a mortar followed by sublimation-condensation). The starting powders were mixed in a ratio of 1: 1 by weight, ground in an agate mortar, and then dried under vacuum at a temperature of 120 ° C to remove water. After that, the mixture of phosphorus and Ketjenblack EC300J was transferred into a glove box with argon atmosphere (Spectroscopic Systems LLC, Russia) and placed in a sealed stainless steel capsule. The water and oxygen content in the box were less than 1 ppm. The capsule was kept in a tubular furnace at a temperature of 600–670 °C for two hours. Next, the furnace was gradually cooled to room temperature for eight hours. Thus, the heat treatment was drastically shortened in comparison with [13−17].

The structure of the initial materials as well as P@KB-EC300J composite was characterized by powder X-ray diffraction (X-ray Powder Diffractometer Huber G670 with Co tube). The microstructure and particle morphology of the as-prepared composite, as well as its elemental composition were observed on a JEOL JSM 6490 LV scanning electron microscope (SEM) with an INCA energy dispersive X-ray analyzer (EDX). Raman spectra were recorded using a DXRxi Raman Imaging Microscope (Thermo Fisher Scientific).

2.2 Preparation of electrodes and assembly of electrochemical cells.

To make the electrodes, the synthesized phosphorus-carbon composite (P@KB-EC300J) was mixed with an aqueous solution of carboxymethyl cellulose in the ratio (9:1, wt.%), then was mixed and ultrasonically homogenized (Sonics Vibra Cell, USA). The resulting paste was applied to stainless steel current-collectors, dried in an oven at a temperature of 80 °C and then dried under vacuum at a temperature of 120 °C for 8 hours to remove traces of water. Electrochemical measurements were carried out in sealed three-electrode cells of a plane-parallel design. The auxiliary and reference electrodes were made of metallic sodium rolled onto a current-collectors of nickel foil. The area of the electrodes was 4.5 cm^2. The load of active substance (P) on the electrode was 1.4–1.5 mg cm^{-2}. Electrochemical cells were assembled in the glove box. A 1 M NaClO$_4$ solution in a mixture of propylene carbonate and ethylene carbonate (1: 1, vol.) was used as an electrolyte. The water content in the electrolyte, measured using a titrator (917 Coulometer, Metrohm) was not more than 15 ppm.

2.3 Electrochemical testing.

The charge (sodium insertion) and discharge (sodium extraction) capacity were recorded using a multi-channel computer-aided cycler AZVRIK-50-10V (Buster JSC, Russia). Cyclic voltammograms were recorded using a multichannel potentiostat P20-X8 (Russia, Elins).

3. RESULTS AND DISCUSSIONS

3.1 Structure and morphology of the as-prepared P@KB-EC300J.

Figure 1 shows the diffraction patterns of red phosphorus, Ketjenblack EC300J and synthesized P@KB-EC300J composite. By and large these diffraction patterns are in good agreement with the results reported in [3, 4, 20, 27] and indicate the formation of a phosphorus composite with carbon.
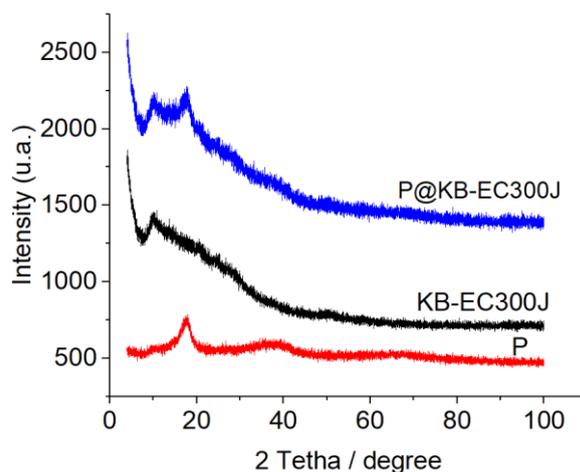

Figure 1. The diffraction patterns of red phosphorus, Ketjenblack EC300J and synthesized P@KB-EC300J composite.

The results of scanning electron microscopy show that the morphology of the synthesized composite is determined by the morphology of the initial Ketjenblack EC300J and represents agglomerated particles from 1 to 5 μm in size, although much large agglomerates are seen as well. (Fig. 2).

The spectrum of energy-dispersive X-ray analysis shows clear peaks corresponding to carbon, phosphorus, and oxygen (Fig. 3).
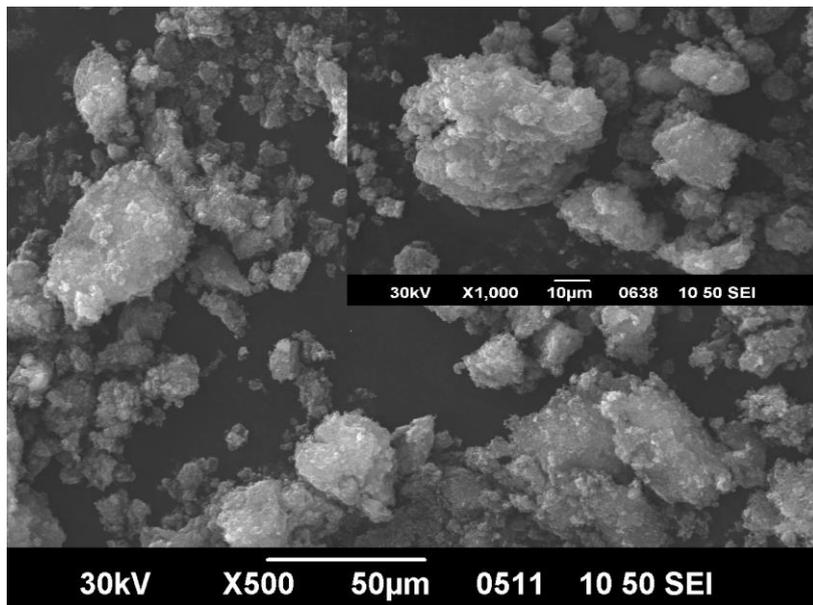
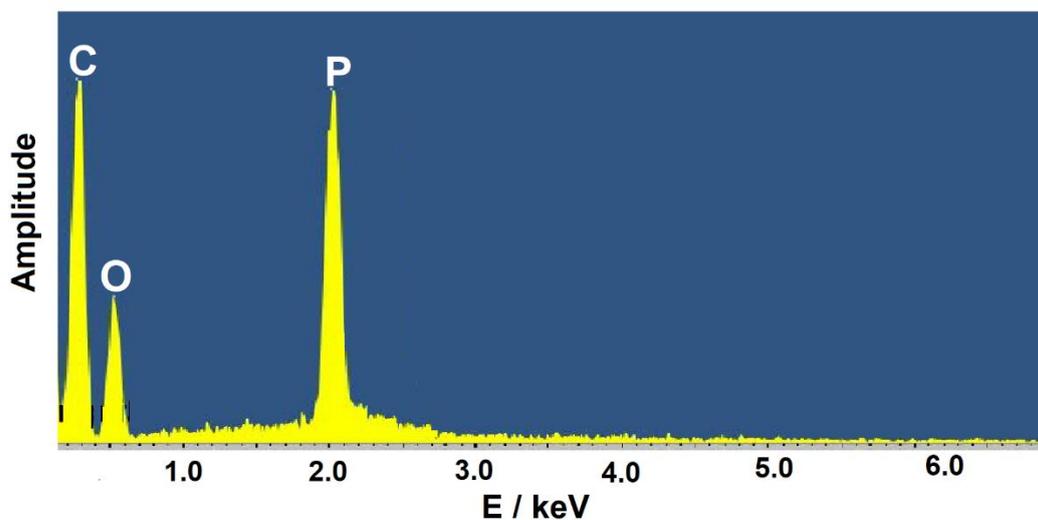**Figure 2.** SEM image of P@KB-EC300J composite.

Figure 3. EDX spectrum of the P@KB-EC300J composite.

Raman spectra of plain Ketjenblack EC300J, and P@KB-EC300J composite are shown in Fig. 4. Both spectra contain well-definite peaks at ca. 1340 and 1580 cm^{-1}, intrinsic to carbon black (D-band and G-band, correspondingly). Spectrum for P@KB-EC300J composite contains also group of weaker peaks near 350 cm^{-1}, corresponding to red phosphorus. It is worth noting that Figure 4 well agrees with data of [5, 6, 15, 28], and evidences the formation certain composite of phosphorus with carbon black.
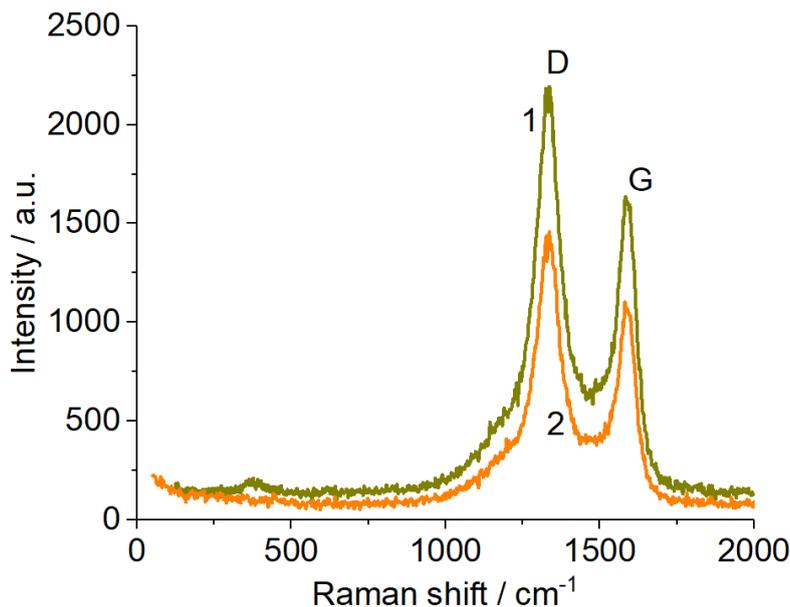
Figure 4. Raman spectra of P@KB-EC300J composite (1), and plain Ketjenblack EC300J (2)

3.2 Galvanostatic cycling.

Figure 5a demonstrates galvanostatic charge-discharge curves, obtained with C-rates from C/20 (125 mA g^{-1}) to 10C (25 A g^{-1}). Two well-definite plateaus corresponding to sodium insertion/extraction are shown at the curves recorded at minimal current density of 125 mA g^{-1}. In this case the discharge capacity amounted to 1870 mAh g^{-1}. Increase of current resulted in diminishing discharge capacity and smoothing these clear plateaus. The discharge capacity at current densities of 0.5, 2.5, 5, 10, 20, and 25 A g^{-1} was equal to 1375, 1085, 720, 505, 355, and190 mAh g^{-1}, correspondingly. The dependence of discharge capacity on C-rate is shown in Figure 5b. This Figure evidence also quite low degradation upon cycling. Close results are reported in [4, 5, 18, 29].
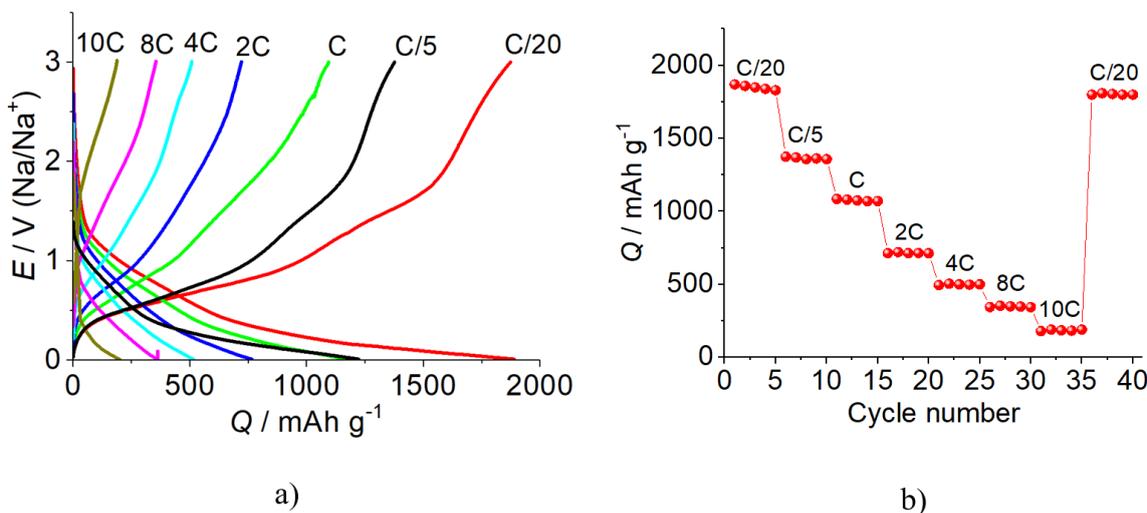

a)   b)

Figure 5. Galvanostatic charge-discharge curves (a) and variation of discharge capacity at cycling with different C-rates (b).

C-rate dependence of discharge capacity Q of batteries is often described with well-known Peukert equation

$$Q = \frac{k}{i^\alpha},\qquad\qquad\qquad\qquad\qquad (2)$$

where i is the current, k is a constant, and exponent α usually falls in the range from 0.2 to 0.7. Surely, this equation is valid only for not too low currents, when Q is independent on i, and formally $\alpha = 0$. Figure 6 shows the Q vs. i dependence for P@KB-EC300J composite in bi-logarithmic coordinates. Some data from the literature are included in this Figure too. One can see that the Peukert equation is hardly valid in this case, in order words the exponent α varies with current variation. At the same time, the results of the present work correspond to some literature data.
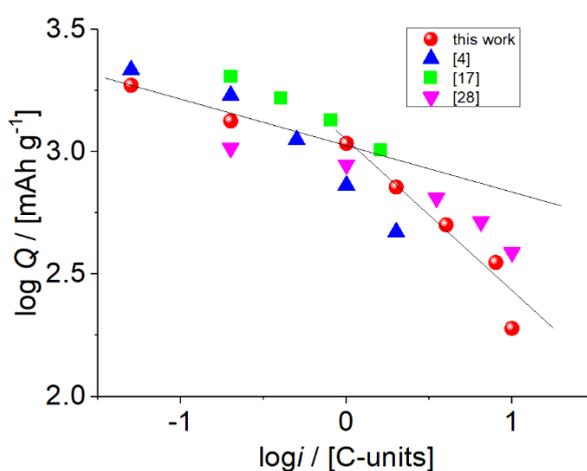

Figure 6. Q vs. i dependences for galvanostatic discharge. Circles – the present work, triangles – data from [4], squares – data from [18], stars – data from [29]

It seems worthwhile to compare the performances of the composite prepared in the present work with literature data on similar composites synthesized via sublimation-condensation method. Such a comparison is presented in Table 1. It is seen that although the synthesis method used in the present study was not so complicated as in the most of quoted works, the results obtained here are mostly superior to literary data.

3.3 Cyclic voltammetry.

Figure 7 presents cyclic voltammograms (CVs) recorded at various potential scan rates. The CVs are in fairly good agreement with galvanostatic curves. There are distinct cathodic and anode maxima in CVs, those correspond to plateaus in galvanostatic curves (Fig. 5). At the same time, the CVs in Fig. 7 qualitatively coincide with CVs presented in [5, 6, 14]. The cathodic maxima at the potentials ca. 0.6 and 0.02 V correspond to sodium insertion into the composite, and anodic ones at the potentials 0.8 and about 2.0 V correspond to sodium extraction from the composite. The irreversible maximum of the current in the potential range 1.1–1.4 V, recorded in the first cycle at a potential scan rate of 0.1 mV

s^{-1}, is associated with the formation of a solid electrolyte film on the composite surface (so-called solid-electrolyte interphase), which was also noted by the authors [14]. An increase in the potential scan rate leads to an increase in current and a shift of the cathodic maxima in the negative direction and anodic maxima in the positive direction.

Table 1. The comparison of performances of P@KB-EC300J composite with literature data

No.	Discharge capacity, mAh g^{-1}	Current, mA g^{-1} or rate (C)	References
1	700	50 mA g^{-1}	13
2	850	100 mA g^{-1}	14
3	1500	C/10	15
4	900	0.6C	16
5	400	25 mA g^{-1}	21
6	1100	100 mA g^{-1}	22
7	900	50 mA g^{-1}	23
8	700	300 mA g^{-1}	24
9	1500	200 mA g^{-1}	25
10	1300	130 mA g^{-1}	26
11	1870	C/20	The present work

The dependence of currents in the anodic maxima in the CVs on the square root of the potential scan rate is linear and passes through the origin (insert in Fig. 7), which points to the diffusion control of the sodium extraction from P@KB-EC300J composite. With this fact in mind, we can calculate the effective diffusion coefficient (*D*) of sodium in the composite with using Randles–Ševcik equation:

$$D^{\frac{1}{2}} = i_p / (2.69 \cdot v^{\frac{1}{2}} \cdot 10^5 S \cdot c \cdot n^{\frac{2}{3}}). \tag{3}$$

Here i_p is a peak current (A), v is the potential scan rate (V s^{-1}), S is the true area of the electrode surface (cm^2), and c is the concentration of sodium ions [mol cm^{-3}], n is number of electrons transferred by one diffusing particle.
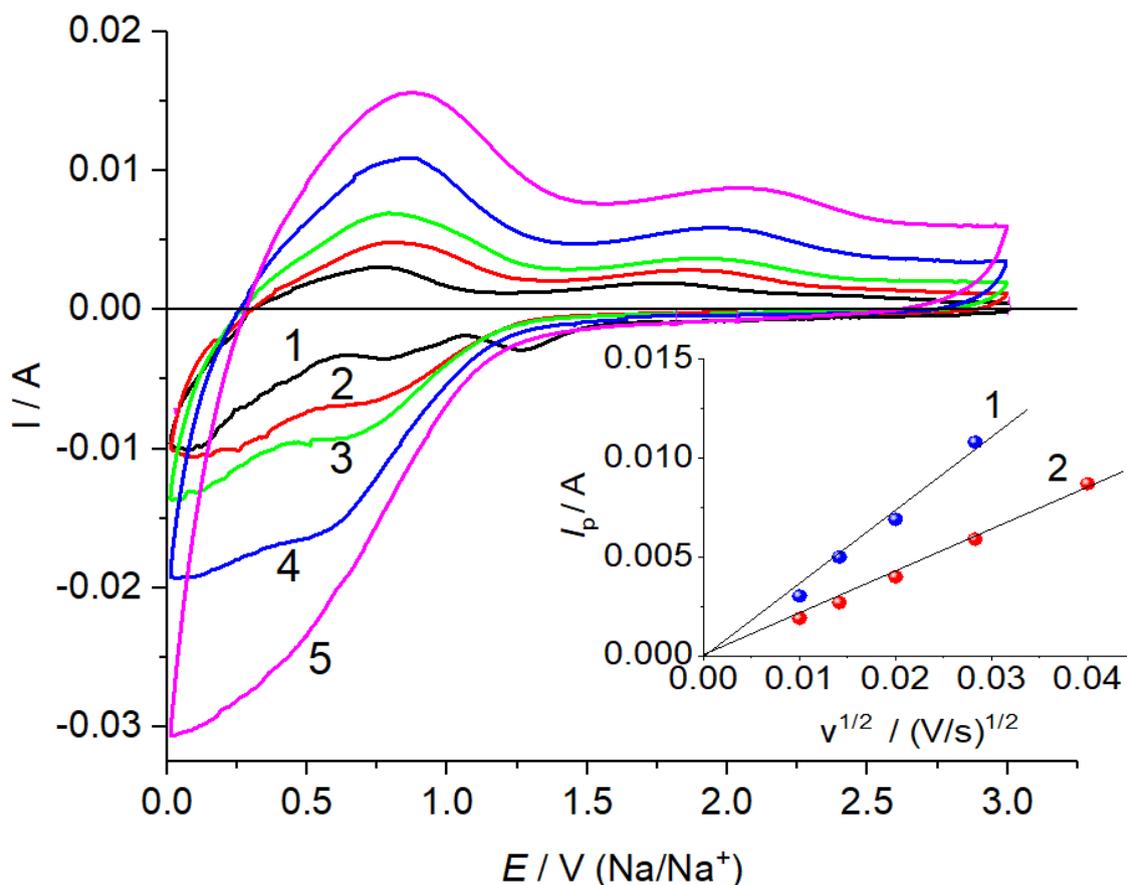
Figure 7. The cyclic voltammograms for the P@KB-EC300J composite at scan rates: 0.1 (1), 0.2 (2), 0.4 (3), 0.8 (4) and 1.6 (5) mV s^{-1}. Insert shows the dependence of current in the anodic maxima in the region I (1), and in the region II (2) on square root from potential scan rate.

For the potential range from 0 to 1.5 V (hereinafter referred to as region I), the sodium ions concentration was 0.135 mol cm^{-3}, for the potential range from 1.5 to 3.0 V (hereinafter, region II), the sodium ions concentration was 0.068 mol cm^{-3}. The slope $di_p/dv^{1/2}$ amounts to 0.37 As$^{1/2}$/V$^{1/2}$ for the region I and to 0.21 As$^{1/2}$/V$^{1/2}$ for the region II. True surface area of the composite particles was calculated according obvious equation:

$$S = 3m/\rho R ,\qquad\qquad\qquad\qquad (4)$$

where m is the composite mass, ρ is density of the composite (2.65 g cm^{-3}), and R is average radius of agglomerated particle (1 μm). The so calculated surface area is equal to 68 cm^2.

The calculation according eq. (3) gives effective diffusion coefficient values $2*10^{-14}$ and $3*10^{-14}$ cm^2 s^{-1} for the regions I and II, correspondingly. Surely, these values are very approximate, mainly due to the large error in the estimate of the true surface area.

The effective diffusion coefficient of alkali metals in the solid phase is known to be from 10^{-17} to 10^{-9} cm^2 s^{-1}. Literary data on the measuring the diffusion coefficient of sodium are few and far between. Thus, the authors of [30] estimated the diffusion coefficient of sodium in sodium vanadium phosphate, which turned out to be 10^{-11} cm^2 s^{-1}. According to the authors of [31], the diffusion coefficient

of sodium in germanium is $3.6*10^{-7}$ cm^2 s^{-1}. The diffusion coefficient of sodium in carbon nanoribbons falls in the range from $5.85*10^{-12}$ to $2.11*10^{-11}$ cm^2 s^{-1} depending on the type of carbon material [32]. According to the authors of [33], the diffusion coefficient of sodium in bismuth ranged from 10^{-14} to 10^{-11} cm^2 s^{-1}, depending on the sodium concentration. The diffusion coefficient of sodium in a nanowire from iron phosphide was estimated by the authors of [34] as 10^{-12} cm^2 s^{-1}. Thus, the value of diffusion coefficient obtained in the present work seems to be wise, although, rather approximate.

4. CONCLUSION

The combined method of synthesis of phosphorus composite with carbon black allowed to obtain a high-performance negative electrode for sodium-ion battery. This composite was prepared from powders of commercial red phosphorus and Ketjenblack EC300J by grinding in a mortar followed by sublimation-condensation. The composite was attested by X-ray diffractometry, scanning electron microscopy, energy-dispersive X-ray analysis, and Raman spectroscopy. The electrode from such a composite were tested with galvanostatic cycling and cyclic voltammetry. The electrode delivered the discharge capacity 1870 mAh g^{-1} at C/20 and 190 mAh g^{-1} at 10C. The sodium effective diffusion coefficient in the composite was estimated as $(3-4)*10^{-14}$ cm^2 s^{-1}.

References

1. Y. Kim, Y. Park, A. Choi, N.S. Choi, J. Kim, J. Lee, J.H. Ryu, S.M. Oh, K.T. Lee, *Adv. Mater.* 25 (2013) 3045.
2. J.M. Sangster, *J. Phase Equilib. Diffus.*, 31(2010) 62.
3. J. Qian, X. Wu, Y. Cao, X. Ai, H. Yang, *Angew. Chem. Int. Ed.*, 52 (2013) 4633.
4. J. Song, Z. Yu, M.L. Gordin, S. Hu, R. Yi, D. Tang, T. Walter, M. Regula, D. Choi, X. Li, A. Manivannan, D. Wang, *Nano Lett.*, 14 (2014) 6329.
5. N. Feng, X. Liang, X. Pu, M. Li, M. Liu, Z. Cong, J. Sun, W. Song, W. Hu, *J. Alloys and Compounds,* 775 (2019) 1270.
6. W.J. Li, S.L. Chou, J.Z. Wang, H.K. Liu, S.X. Dou, *J. Mater. Chem. A,* 4 (2016) 505.
7. G.H. Lee, M.R. Jo, K. Zhang, Y.M. Kang, *J. Mater. Chem. A,* 5 (2017) 3683.
8. J. Song, Z. Yu, M.L. Gordin, X. Li, H. Peng, D. Wang, *ACS Nano,* 9 (2015) 11933.
9. W. Liu, X. Yuan, X. Yu, *Nanoscale,* 10 (2018) 16675.
10. W.J. Li, S.L. Chou, J.Z. Wang, H.K. Liu, S.X. Dou, *Nano Lett.,* 13 (2013) 5480.
11. C. Marino, A. Debenedetti, B. Fraisse, F. Favier, L. Monconduit, *Electrochem. Comm.*, 13 (2011) 346.
12. L. Wang, X. He, J. Li, W. Sun, J. Gao, J. Guo, C. Jiang, *Angew. Chem. Int. Ed.,* 51 (2012) 9034.
13. Z. Zhu, Y. Wen, X. Fan, T. Gao, F. Han, C. Luo, S.C. Liou, C. Wang, *ACS Nano,* 9 (2015) 3254.
14. B. Ruan, J. Wang, D. Shi, Y. Xu, S. Chou, H. Liu, J. Wang, *J. Mater. Chem. A,* 3 (2015) 19011.

15. J. Xu, J. Ding, W. Zhu, X. Zhou, S. Ge, N. Yuan, *Sci. China Mater.*, 61 (2018) 371.
16. W. Li, Z. Yang, M. Li, Y. Jiang, X. Wei, X. Zhong, L. Gu, Y. Yu, *Nano Lett.*, 16 (2016) 1546.
17. Z. Yu, J. Song, D. Wang, D. Wang, *Nano Energy*, 40 (2017) 550.
18. L. Pei, Q. Zhao, C. Chen, J. Liang, J. Chen, *ChemElectroChem*, 2 (2015) 1652.
19. H. Gao, T. Zhou, Y. Zheng, Y. Liu, J. Chen, H. Liu, Z. Guo, *Adv. Energy Mater.*, 6 (2016) Article No. 1601037.
20. Y. Liu, A. Zhang, C. Shen, Q. Liu, X. Cao, Y. Ma, L. Chen, C. Lau, T.C. Chen, F. Wei, C. Zhou, *ACS Nano*, 11 (2017) 5530.
21. N. Wu, H.R. Yao, Y.X. Yin, Y.G. Guo, *J. Mater. Chem. A,* 3, (2015) 24221.
22. Y. Wu, Z. Liu, X. Zhong, X. Cheng, Z. Fan, Y. Yu, *Small*, 14 (2018) Article No. 1703472.
23. X. Ma, L. Chen, X. Ren, G. Hou, L. Chen, L. Zhang, B. Liu, Q. Ai, L. Zhang, P. Si, J. Lou, J. Feng, L. Ci, *J. Mater. Chem. A*, 6 (2018) 1574.
24. W. Li, S. Hu, X. Luo, Z. Li, X. Sun, M. Li, F. Liu, Y. Yu, *Adv. Mater.*, 29 (2017) Article No. 1605820.
25. C. Zhang, X. Wang, Q. Liang, X. Liu, Q. Weng, J. Liu, Y. Yang, Z. Dai, K. Ding, Y. Bando, J. Tang, D. Golberg, *Nano Lett.*, 16 (2016) 2054.
26. J. Li, L. Wang, Z. Wang, G. Tian, X. He, *ACS Omega*, 2 (2017) 4440.
27. Y. Wang, L. Tian, Z. Yao, F. Li, S. Li, S. Ye, *Electrochim. Acta*, 163 (2015) 71.
28. W. Tian, L. Wang, K. Huo, X. He, *J. Power Sources*, 430 (2019) 60.
29. J. Sun, H.W. Lee, M. Pasta, Y. Sun, W. Liu, Y. Li, H.R. Lee, N. Liu, Y. Cui, *Energy Storage Materials*, 4 (2016) 130.
30. Essehli R, Yahia HB, Amin R, El-Mellouhi F, Belharouak I. Selective sodium-ion diffusion channels in $Na_{2-x}Fe_3(PO_4)_3$ positive electrode for Na-ion batteries. *Energy Storage Materials*. (2019) https://doi.org/10.1016/j.ensm.2019.07.040 [accepted for publication, available on-line 30 July 2019]
31. G.S. Pekar, A.F. Singaevsky, *Mater. Sci. Semicond. Proces.*, 64 (2019) 10.
32. B. Jiang, Y. Zhang, D. Yan, J.L. Xia, W.C. Li, *ChemElectroChem*, 6 (2019) 3043.
33. C. Wang, D. Du, M. Song, Y. Wang, F. Li, *Adv. Energy Mater.*, 9 (2019) Article 1900022.
34. L. Wang, X. Zhao, S. Dai, Y. Shen, M. Wang, *Electrochim. Acta*, 314 (2019) 142.